AIAA JOURNAL
Vol. 36, No. 3, March 1998

Scaling of Equilibrium Boundary Layers Under Adverse Pressure Gradient Using Turbulence Models

Ruud A. W. M. Henkes*
Delft University of Technology, 2629 HS Delft, The Netherlands

The large Reynolds number behavior of four commonly used turbulence models was investigated by numerically solving the boundary-layer equations up to $Re_\theta = 10^8$ for turbulent boundary layers under an adverse pressure gradient with an equilibrium parameter $\beta = (\delta^*/\tau_w)(dp/dx)$ in the range between 0 and 200. All models reproduce the same classical scalings in the inner and outer layer. The solution in the outer layer asymptotes to the defect law described by the defect-layer equation as derived by Tennekes and Lumley (Tennekes, H., and Lumley, J. L., *A First Course in Turbulence*, MIT Press, Cambridge, MA, 1972, pp. 186–188) and not to the one derived by Wilcox (Wilcox, D. C., *Turbulence Modeling*, DCW Industries, Inc., La Cañada, CA, 1993, pp. 110–121). The asymptotic state is obtained at a higher Reynolds number for increasing β value. The turbulence models show that the same outer-edge velocity can generate two different equilibrium boundary layers. Comparison with existing experiments shows that the differential Reynolds stress model is very accurate; the algebraic model and the k–ω model are also reasonably good. The k–ϵ model is not accurate for these adverse-pressure gradient boundary layers, and it gives a far too large wall-shear stress.

Introduction

THE present study derives the scalings according to four commonly used turbulence models for equilibrium boundary layers under an adverse pressure gradient. According to Clauser,[1] the boundary layer is in equilibrium if the parameter $\beta = (\delta^*/\tau_w)(dp/dx)$ is independent of the streamwise coordinate, or equivalently, independent of the local Reynolds number $Re_\theta = U\theta/\nu$ (with U the outer edge velocity, θ the momentum thickness, and ν the kinematic viscosity). The proper scalings are those that cause the scaled flow to become independent of the local Reynolds number, when its value has become sufficiently large. The scaled flow can then also be referred to as a similarity flow type. The similarity scalings and corresponding velocity and turbulence profiles are of great theoretical and practical interest. When the flow is independent of its streamwise coordinate, a theoretical model, e.g., a turbulence model, needs to be compared with experimental data at a single streamwise position only. In applications knowledge of the scalings can direct the upscaling of laboratory experiments to real-life configurations, such as wind-tunnel tests for the drag of airfoils and aircraft vs real in-flight drag.

The scalings are derived from the turbulence models without making any additional a priori assumptions, which means that the scalings follow from the straightforward numerical solution of the boundary-layer equations. Computations are made up to the very large Reynolds number of $Re_\theta = 10^8$, which is sufficient for the similarity scalings to appear. A strong grid refinement was applied close to the wall. By doubling the number of grid points, the solutions were verified to be numerically accurate.

The classical theory, e.g., due to Clauser,[1] von Kármán,[2] Millikan,[3] and Coles,[4] finds that the boundary layer can be split up in an inner layer (law of the wall), with length scale ν/u_τ and velocity scale u_τ, and an outer layer (defect layer), with the velocity scale u_τ and the length scale $\Delta = \delta^*(U/u_\tau)$ (where δ^* denotes the displacement thickness and u_τ the wall-shear stress velocity). For large y^+, i.e., (yu_τ/ν), the theory predicts the logarithmic shape of the law of the wall. Furthermore, $u_\tau/U \to 0$ for $Re_\theta \to \infty$. Recently, George and Castillo[5] have doubted the correctness of the classical theory, and instead they propose a power-law dependence for the law of the wall and a nonzero constant for u_τ/U at large Reynolds number. The latter proposal has been received, however, with some skepticism by the fluid-mechanics community.

The purpose of this study is threefold.

1) Find the proper scalings in the inner and outer layer according to four commonly used types of turbulence models of increasing complexity: the algebraic model of Cebeci and Smith,[6] the two-equation k–ϵ model of Launder and Sharma,[7] the two-equation k–ω model of Wilcox,[8] and the differential Reynolds stress model of Hanjalić et al.[9]

2) Verify whether the solution in the defect layer as predicted by the boundary-layer equations equals either the solution of the defect-layer equation proposed by Wilcox[8] or the one proposed by Tennekes and Lumley.[10] There is a difference between the formulations, and only one of the two can be correct.

3) Compare the performance of the different turbulence models with experiments, including the new data set obtained by Skåre[11] and Skåre and Krogstad[12] for the equilibrium boundary layer at $\beta = 20$, which is close to turbulent separation.

Theory for the Scalings of the Inner and Outer Layer

To derive the scalings of the boundary layer under an adverse pressure gradient we start from the turbulent boundary-layer equations for an incompressible flow, which read

$$\frac{\partial u}{\partial x} + \frac{\partial v}{\partial y} = 0 \tag{1}$$

$$u\frac{\partial u}{\partial x} + v\frac{\partial u}{\partial y} = -\frac{1}{\rho}\frac{dp}{dx} + \nu\frac{\partial^2 u}{\partial y^2} - \frac{\partial}{\partial y}\overline{u'v'} \tag{2}$$

where x and y are the coordinates along and normal to the wall, respectively; u and v are the corresponding velocity components; p is the pressure; ρ is the density; ν is the kinematic viscosity; and $-\overline{u'v'}$ is the Reynolds shear stress.

According to the classical theory, which is mainly due to Clauser[1] and Coles,[4] the velocity scale in both the inner and outer layer is the same, namely, u_τ, which is the wall-shear stress velocity $(\tau_w/\rho)^{1/2}$, with τ_w the wall-shear stress $\mu(\partial u/\partial y)_w$. The length scale differs and is ν/u_τ for the inner layer and $\Delta = \delta^* U/u_\tau$ for the outer layer; δ^* is the displacement thickness and U is the local outer-edge velocity. Among others, Tennekes and Lumley[10] and Wilcox[8] have derived a so-called defect-layer equation, which is the equation that describes the similarity solution in the outer layer. As the present author noticed a striking difference between the derivations of Tennekes and Lumley and of Wilcox, implying that one of the two equations is not correct, the theory is discussed here.

Received Jan. 28, 1997; revision received Sept. 19, 1997; accepted for publication Oct. 1, 1997.

*Senior Researcher, Faculty of Aerospace Engineering; currently Research Engineer, Department of Fluid Flow and Thermodynamics, Shell International Oil Products B.V., P.O. Box 38000, 1030 BN Amsterdam, The Netherlands. E-mail: ruud.a.w.m.henkes@opc.shell.com.

It is assumed that molecular diffusion can be neglected in the outer layer, which simplifies the boundary-layer equations (1) and (2) to

$$\frac{\partial u}{\partial x}+\frac{\partial v}{\partial y}=0 \tag{3}$$

$$u\frac{\partial u}{\partial x}+v\frac{\partial u}{\partial y}=-\frac{1}{\rho}\frac{\mathrm{d}p}{\mathrm{d}x}-\frac{\partial}{\partial y}\overline{u'v'} \tag{4}$$

The (x, y) coordinates are transformed into (ξ, η) coordinates, according to $\xi = x$ and $\eta = y/\Delta$, where Δ is the length scale of the boundary layer. The velocity and Reynolds stress are scaled as $(U-u)/U_0 = f(y/\Delta)$ and $(-\overline{u'v'})/R_0 = r(y/\Delta)$, where U_0 is a proper velocity scale, and R_0 is a proper velocity scale squared. Transformation of the momentum equation (4) gives

$$\left(-\frac{U}{U_0}\frac{\Delta}{U_0}\frac{\mathrm{d}U_0}{\mathrm{d}\xi}-\frac{\Delta}{U_0}\frac{\mathrm{d}U}{\mathrm{d}\xi}\right)f+\left(\frac{\Delta}{U_0}\frac{\mathrm{d}U_0}{\mathrm{d}\xi}\right)f^2+\left(\frac{U}{U_0}\frac{\mathrm{d}\Delta}{\mathrm{d}\xi}+\frac{\Delta}{U_0}\frac{\mathrm{d}U}{\mathrm{d}\xi}\right)\eta f'-\left(\frac{\mathrm{d}\Delta}{\mathrm{d}\xi}+\frac{\Delta}{U_0}\frac{\mathrm{d}U_0}{\mathrm{d}\xi}\right)f'\int_0^\eta f\,\mathrm{d}\eta=\frac{R_0}{U_0^2}r' \tag{5}$$

A prime denotes differentiation to η.

Substituting the classical scalings ($U_0 = u_\tau$, $\Delta = \delta^* U/u_\tau$, $R_0 = u_\tau^2$) into Eq. (5) gives

$$(\beta-2\omega)f+\gamma f^2+(\alpha-2\beta-2\omega)\eta f'-\chi f'\int_0^\eta f\,\mathrm{d}\eta=r' \tag{6}$$

with

$$\alpha=\left(\frac{U}{u_\tau}\right)^2\frac{\mathrm{d}\delta^*}{\mathrm{d}\xi},\qquad \beta=\frac{\delta^*}{\tau_w}\frac{\mathrm{d}p}{\mathrm{d}x},\qquad \omega=\frac{1}{2}\frac{\delta^*}{u_\tau}\left(\frac{U}{u_\tau}\right)^2\frac{\mathrm{d}u_\tau}{\mathrm{d}\xi} \tag{7}$$

$$\gamma=\frac{U}{u_\tau}\frac{\delta^*}{u_\tau}\frac{\mathrm{d}u_\tau}{\mathrm{d}\xi},\qquad \chi=\frac{U}{u_\tau}\frac{\mathrm{d}\delta^*}{\mathrm{d}\xi}+\frac{\delta^*}{u_\tau}\frac{\mathrm{d}U}{\mathrm{d}\xi}$$

If Eq. (6) defines a similarity equation, the coefficients α, β, ω, γ, and χ must become constants for $Re_\theta \to \infty$. As shown subsequently, this is indeed the case.

Approaching the wall, the solution in the outer layer must match with the solution in the inner layer. If one assumes that convection can be neglected close to the wall, the boundary-layer equations (1) and (2) for the inner layer reduce to

$$\frac{\partial u}{\partial x}+\frac{\partial u}{\partial y}=0 \tag{8}$$

$$0=\frac{1}{\rho}\frac{\mathrm{d}p}{\mathrm{d}x}+\nu\frac{\partial^2 u}{\partial y^2}-\frac{\partial}{\partial y}\overline{u'v'} \tag{9}$$

Nondimensionalization of the momentum equation with the velocity scale u_τ and the length scale ν/u_τ (and denoting scaled quantities with the common + superscript) gives

$$0=\frac{\beta}{Re^*}+\frac{\partial^2 u^+}{\partial y^{+2}}-\frac{\partial}{\partial y^+}\overline{u'v'}^+ \tag{10}$$

Here Re^* is the local Reynolds number defined by $u_\tau\delta^*/\nu$. The equation shows that the pressure contribution can be neglected if local Reynolds number becomes increasingly large. The stronger the adverse pressure gradient (giving larger β), the larger local Reynolds number must be to justify the neglect of the pressure term in the inner layer. At separation (giving $\beta/Re^* \to \infty$) the pressure contribution cannot be neglected. In the present study, though β could be as large as 20 or even 200, separation itself is not considered, but the local Reynolds number is increased instead.

If the pressure can be neglected, the same law of the wall holds in the inner layer for boundary layers with and without streamwise pressure gradient. Using the boundary conditions $u^+ = \overline{u'v'}^+ = 0$ at $y^+ = 0$, the inner-layer equation gives

$$\lim_{y^+\to\infty} -\overline{u'v'}^+ = 1 \tag{11}$$

and

$$\lim_{y^+\to\infty} u^+ = (1/\kappa)\ell_n(y^+)+C \tag{12}$$

The latter expression can be rewritten in outer-layer scalings as

$$\lim_{\eta\to 0}[(U-u)/u_\tau] = f(\eta) = -(1/\kappa)\,\ell_n(\eta)+C' \tag{13}$$

This equation can be used as a boundary condition to solve Eq. (6).

Eliminating u from Eqs. (12) and (13) gives the following wall-shear stress law:

$$c_f = 2\left(\frac{u_\tau}{U}\right)^2 = \frac{2}{[C+C'+(1/\kappa)\,\ell_n Re_{\delta^*}]^2} \tag{14}$$

with $Re_{\delta^*} = U\delta^*/\nu$. This shows that $u_\tau/U \to 0$ for $Re_{\delta^*} \to \infty$ and, thus, for $Re_\theta \to \infty$. To find the asymptotic values of Eq. (7), these coefficients are developed in a series with respect to the small parameter u_τ/U. Use is made of the integral form of the momentum equation (2), which reads

$$\frac{\mathrm{d}\theta}{\mathrm{d}x}-(2+H)\frac{\theta}{\rho U^2}\frac{\mathrm{d}p}{\mathrm{d}x}=\frac{c_f}{2} \tag{15}$$

where the wall-shear stress coefficient is defined as $c_f = \tau_w/\frac{1}{2}\rho U^2 = 2(u_\tau/U)^2$. This equation is equivalent to

$$\alpha\frac{\mathrm{d}\theta}{\mathrm{d}x}=\left(1+\frac{2+H}{H}\beta\right)\frac{\mathrm{d}\delta^*}{\mathrm{d}x} \tag{16}$$

Use is also made of the definitions of δ^* and θ. For δ^* we have

$$\delta^* = \int_0^\infty\left(1-\frac{u}{U}\right)\mathrm{d}y = \delta^*\int_0^\infty f\,\mathrm{d}\eta \tag{17}$$

Hence, the definition of δ^* leads to the integral restriction

$$\int_0^\infty f\,\mathrm{d}\eta = 1 \tag{18}$$

The definition of θ gives

$$\theta=\int_0^\infty\frac{u}{U}\left(1-\frac{u}{U}\right)\mathrm{d}y=\int_0^\infty\left(1-\frac{u_\tau}{U}f\right)f\delta^*\,\mathrm{d}\eta$$

$$=\delta^*\left(1-C^*\frac{u_\tau}{U}\right) \tag{19}$$

with

$$C^* = \int_0^\infty f^2\,\mathrm{d}\eta$$

According to Eq. (19), the shape factor can be expressed as

$$1/H = \theta/\delta^* = 1-C^*(u_\tau/U) \tag{20}$$

As $u_\tau/U \to 0$ for $Re_\theta \to \infty$, this relation shows that $H \to 1$ for very large Reynolds numbers. It is noted that C^* is the same as the so-called Clauser parameter G, which can be used as an alternative for β to denote that the boundary layer has reached an equilibrium state. Using Eq. (19), we have

$$G=\int_0^\infty\left(\frac{U-u}{u_\tau}\right)^2\mathrm{d}\left(\frac{y}{\Delta}\right)=\frac{1-(1/H)}{(c_f/2)^{\frac{1}{2}}} \tag{21}$$

Substitution of Eq. (14) into Eq. (7) and applying Eqs. (16) and (20) gives the following series expansion of the coefficients (7):

$$\alpha = 1+3\beta+(1+\beta)C^*(u_\tau/U)+\cdots$$

$$\omega = -\tfrac{1}{2}\beta-(1/2\kappa)(1+2\beta)(u_\tau/U)+\cdots \tag{22}$$

$$\gamma = -\beta(u_\tau/U)-(1/\kappa)(1+2\beta)(u_\tau/U)^2+\cdots$$

$$\chi = (1+2\beta)(u_\tau/U)+\cdots$$

or to leading order $\alpha = 1+3\beta$, $\omega = -\frac{1}{2}\beta$, and $\gamma = \chi = 0$.

Therefore, for increasing Re_θ Eq. (6) asymptotes to the following defect-layer equation for the outer layer:

$$2\beta f + (1+2\beta)\eta f' = r' \tag{23}$$

with boundary conditions $f \to -(1/\kappa)\,\ell n\,\eta + C'$ for $\eta \to 0$, $f \to 0$ for $\eta \to \infty$, and the integral restriction

$$\int_0^\infty f\,d\eta = 1$$

Tennekes and Lumley[10] end up with the same equation, but they did not show the series expansions as has just been given. Wilcox[8] ends up with a different equation,

$$\beta f + (1+\beta)\eta f' = r' \tag{24}$$

He argues that $\omega \to 0$ for $Re_\theta \to \infty$. Substituting this, together with $\alpha = 1+3\beta$ and $\gamma = \chi = 0$, into Eq. (6) gives Eq. (24). However, our systematic series expansion shows that ω does not vanish, but asymptotes to $-\frac{1}{2}\beta$ instead. This proves that Eq. (23) is the correct defect-layer equation, as will also be confirmed by the solutions from the boundary-layer equations, presented in the sequel of this paper. Wilcox's formulation is only correct for the zero pressure gradient case ($\beta = 0$).

Turbulence Models

To solve the boundary-layer equations (1) and (2) or the defect-layer equation (23), a turbulence model is needed to represent the Reynolds shear stress. The following models are considered: algebraic model of Cebeci and Smith,[6] two-equation low-Reynolds-number k–ϵ model of Launder and Sharma,[7] two-equation low-Reynolds-number k–ω model of Wilcox,[8] and differential Reynolds stress model of Hanjalić et al.[9]

The algebraic model uses an algebraic relation to approximate the turbulent viscosity that appears in $-\overline{u'v'} = \nu_t(\partial u/\partial y)$. The k–ϵ model solves differential equations for the turbulent kinetic energy and the turbulent dissipation rate ϵ to model the turbulent viscosity, whereas the k–ω model solves a differential equation for ω instead of ϵ (where ω is proportional to ϵ/k). The differential Reynolds stress model (DSM) is the most complete model, as it solves differential equations for all Reynolds shear and normal stresses, as well as for ϵ. More details of the models are given in the cited references, and in Ref. 13. Within each class of models (algebraic, k–ϵ, k–ω, and DSM) only one specific formulation has been considered here. These formulations are well known in the literature and have already been applied to a number of flow types. However, other formulations might exist (particularly within the class of k–ϵ models) that are more suited for boundary layers under an adverse pressure gradient.

The boundary-layer equations are solved with a marching numerical procedure, after discretization with a second-order finite difference scheme. A Cartesian grid is used with a very strong grid refinement in the lower part of the inner layer. The outer edge of the computational domain was checked to be chosen sufficiently far so as to have a negligible effect on the development of the boundary layer. To account for the growth of the boundary layer in the streamwise direction, at different x positions the outer edge was increased and the y grid points were redistributed. All results presented are guaranteed to be grid independent. This was checked by doubling the number of points in x and y direction. A typical y grid consists of 200 or 400 points.

The defect-layer equation (23) depends on only the single coordinate η. This ordinary differential equation was numerically discretized with a second-order difference scheme, applying 200 or 400 points. An iteration process was used to satisfy the boundary conditions and the integral restriction.

Asymptotic Behavior at Increasing Reynolds Number

The boundary-layer equations were solved for the four turbulence models with different β values between 0 and 200. The calculations were started at $Re_\theta = 300$, where the results from direct numerical simulations by Spalart[14] for a zero-pressure gradient were used as starting profiles. At each downstream position the outer-edge velocity was iteratively updated until the chosen β was obtained. The calculations were extended up to about $Re_\theta = 10^8$.

For all considered models the classical scalings appear for increasing Reynolds number. An example is given in Fig. 1, which shows the velocity and Reynolds shear stress in the inner and outer layer, as obtained with the DSM for $\beta = 1$. In the inertial sublayer, being the outer part of the inner layer, the velocity (Fig. 1a) asymptotes to the logarithmic law of the wall; the generally accepted best fit to experiments (having $\kappa = 0.41$ and $C = 5$) is shown as a long dashed line. The velocity in the outer layer (Fig. 1b), when scaled with u_τ and Δ, asymptotes to a single similarity profile, the so-called defect law. Only the solution for $Re_\theta = 10^3$ shows some deviation from the asymptotic state, but up to at least graphical accuracy no changes are found from $Re_\theta = 10^4$ on. The Reynolds shear stress in the outer part of the inner layer (Fig. 1c) approaches the law of

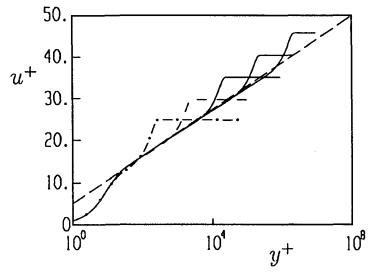

a) Velocity in inner layer (– – –, experimental law of wall)

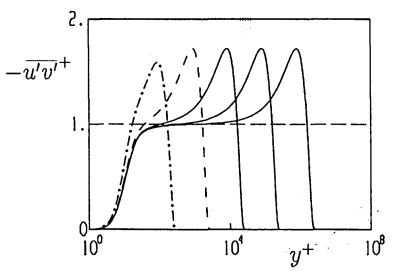

c) Reynolds shear stress in inner layer (– – –, theoretical law of wall for Reynolds shear stress)

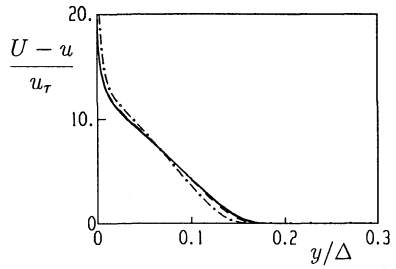

b) Velocity in outer layer

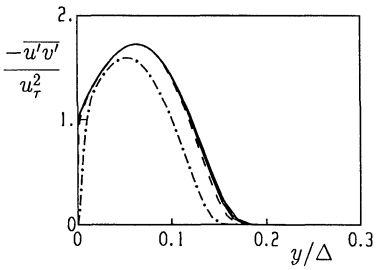

d) Reynolds shear stress in outer layer

Fig. 1 Appearance of the law of the wall and the defect law for increasing Reynolds number according to the DSM with $\beta = 1$; – · –, $Re_\theta = 10^3$; – – –, 10^4; and ——, 10^5, 10^6, and 10^7.

the wall $-\overline{u'v'}^+ = 1$ [Eq. (11)]. The Reynolds shear stress in the outer layer (Fig. 1d) asymptotes to a similarity shape with a local maximum. The appearance of a maximum for the Reynolds shear stress in the outer layer [with $(-\overline{u'v'})/u_\tau^2 > 1$], as well as for the turbulent kinetic energy, is characteristic for adverse pressure gradient boundary layers ($\beta > 0$); such a maximum is not found for the zero pressure gradient boundary layer ($\beta = 0$; see Ref. 15 for more details).

We checked that the similarity profiles for the different quantities in the inner layer are independent of β, which is in agreement with the discussed theory, showing that the same law of the wall holds independent of the pressure gradient. For all four considered turbulence models the scalings for the inner and outer layer are the same. Differences are found for the resulting similarity profiles, some of which are discussed later.

To give some quantitative insight in how the asymptote is obtained for the DSM at $\beta = 1$, Table 1 gives the values for u_τ/U, H, and the coefficients (7) [as appear in the outer-layer equation (6)] for Re_θ increasing from 10^4 to 10^8. The large Reynolds number behavior is in full agreement with the series expansions with respect to u_τ/U, as given by Eq. (22) (with $C^* = G = 8.9$ following from the calculations). This confirms that the solution of the boundary-layer equations asymptotes to the similarity solution described by the defect-layer equation (23) for increasing Reynolds number.

Figure 2 shows the similarity solution for the k–ϵ model at $\beta = 8$, as obtained from the defect-layer equation (23) [Eq. (6) with $\alpha = 25$, $\omega = -4$, $\gamma = \chi = 0$; the solution is denoted as the solid line in Fig. 2] and from the defect-layer equation (24) [Eq. (6) with $\alpha = 25$, $\omega = \gamma = \chi = 0$; denoted as Δ in Fig. 2]. Figure 2 shows that the solution of the boundary-layer equations asymptotes to the solution of the defect-layer equation (23) (given by Tennekes and Lumley[10] and also derived in this paper) and not to Wilcox's[8] defect-layer equation (24). However, even for the Reynolds numbers as large at Re_θ there still is a slight difference (particularly for the Reynolds shear stress in Fig. 2b) between the boundary-layer solution and the defect-layer solution [Eq. (23)]. The reason is that the rate at which the asymptote is approached becomes slower (with respect to Re_θ) for increasing β. The maximum in the Reynolds shear stress for the solution of the boundary-layer equations at $Re_\theta \to \infty$ can be guessed by extrapolating the solution for $Re_\theta = 10^6$ and 10^8, using the series expansion

$$\frac{(-\overline{u'v'})_{\max}}{u_\tau^2} = C_0 + C_1 \frac{u_\tau}{U} + \cdots \tag{25}$$

where C_1 and C_2 are constants, with $C_1 = [(-\overline{u'v'})_{\max}/u_\tau^2]_{Re_\theta \to \infty}$. For $Re_\theta = 10^6$ the maximum is 7.89 (and $u_\tau/U = 0.0231$), and for $Re_\theta = 10^8$ the maximum is 8.05 (and $u_\tau/U = 8.05$). The extrapolation gives $C_1 = 8.75$, which is close to the value 8.81 found with the defect-layer equation (23). As $Re_\theta = 10^8$ can be considered as an upper limit of the range of Reynolds numbers relevant for practical aircraft aerodynamics, it follows from this analysis that a slight error always is made when the defect-layer equation instead of the boundary-layer equations are used to compute the turbulence quantities. The practical relevance of the defect-layer equation thus decreases for increasing adverse pressure gradient, and the boundary-layer equations should be used instead.

Another illustration of the decreasing rate at which the boundary-layer solution asymptotes to the similarity state is given in Fig. 3a, which shows the Reynolds number dependence of the shape factor for the boundary-layer solution at different β values, according to the DSM. All curves reach $H = 1$ at $Re_\theta \to \infty$, but the shape factor at $Re_\theta = 10^8$ for $\beta = 0$, 8, and 20 still is 14, 47, and 71%, respectively, above its asymptotic value.

An interesting practical question is how the outer-edge velocity should be chosen to realize an equilibrium turbulent boundary layer, as represented by a certain constant β value. Bradshaw[16] has suggested that a practically constant β results if the outer-edge velocity is chosen so that $U \propto (x - x_0)^m$ (where x_0 is a virtual origin and m is a constant power). To verify this, we prescribed m and computed β for increasing Re_θ, but β turns out to be very sensitive to m when m comes close to -0.25, that is, where turbulent separation is about to occur. This problem was overcome by prescribing β instead of m. Figure 3b shows the results for the DSM. Here the local m value is defined as $(x/U)(dU/dx)$. The turbulence model does not give a Reynolds number independent m power for equilibrium layers; instead, the power becomes slightly more negative for increasing Reynolds number. As explained by Tennekes and Lumley,[10] this feature also follows from the similarity theory.

Some authors, including Clauser[1] (who measured $\beta \approx 2$ and ≈ 8), have reported difficulties in establishing a stable flow in the wind

Table 1 Re_θ dependence of the coefficients in the defect-layer equation (6) as computed with the DSM for $\beta = 1$

Re_θ	u_τ/U	H	α	ω	γ	χ
10^4	0.0337	1.456	4.73	−0.655	−0.0440	0.125
10^5	0.0285	1.350	4.61	−0.619	−0.0353	0.103
10^6	0.0247	1.287	4.51	−0.605	−0.0299	0.087
10^7	0.0219	1.244	4.44	−0.586	−0.0256	0.075
10^8	0.0196	1.212	4.39	−0.582	−0.0228	0.066
∞	0	1	4	−0.5	0	0

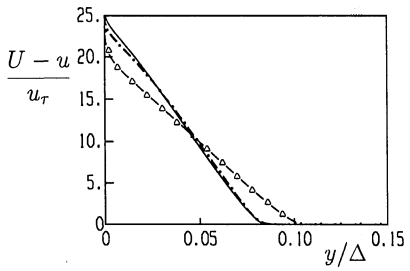

a) Velocity

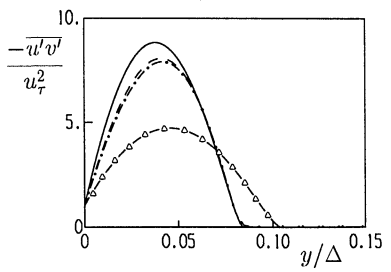

b) Reynolds shear stress

Fig. 2 Comparison between solutions for $\beta = 8$, using the k–ϵ model, obtained with the boundary-layer equations at $Re_\theta = 10^6$ (–·–) and 10^8 (– – –) and with the defect-layer equations (23) (——) and (24) (△).

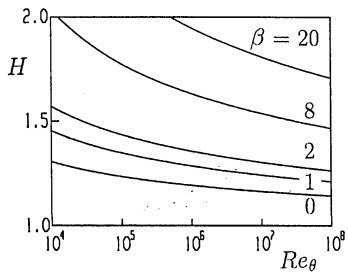

a) Shape factor

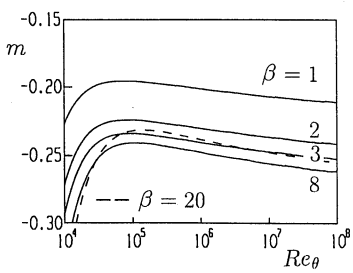

b) Power dependence of the freestream velocity

Fig. 3 Reynolds number dependence of different quantities for equilibrium boundary layers according to the DSM.

tunnel when the adverse pressure gradient becomes stronger. Based on this experience, Clauser suggested that the same outer-edge velocity (represented by the same m value) can correspond with two equilibrium boundary layers, i.e., two β values. This means that an established experimental equilibrium boundary layer can suddenly lose stability and jump to the other flow type. This, indeed, is what is found with the DSM in Fig. 3b. For a given Re_θ (above 10^6) the m power decreases for β values up to about 8, above which the power increases again. For example, the m value for $\beta = 3$ is almost the same as for $\beta = 20$ (for which experiments were performed by Skåre and Krogstad[12]). A similar nonuniqueness is found with the other turbulence models.

Comparison with Experiments

Skåre[11] evaluated experimental data for the Reynolds shear stress at different β values. He noticed that $-\overline{u'v'}_{\max}/u_\tau^2$ becomes proportional to β, for increasing β, but he did not give an explanation. This behavior can be explained with the defect-layer equation (23). For large β, the constant $\alpha = 1 + 3\beta$ can be replaced by $\alpha = 3\beta$. Substituting this and $\tilde{\eta} = \eta\sqrt{\beta}$, $\tilde{f} = f/\sqrt{\beta}$, $\tilde{r} = r/\beta$ into Eq. (23) gives

$$\tilde{f} + \tilde{\eta}\tilde{f}' = \tilde{r}' \tag{26}$$

with the boundary conditions

$$\int_0^\infty \tilde{f}\, d\tilde{\eta} = 1$$

and $\tilde{f} \to 0$ for $\tilde{\eta} \to \infty$. This shows that the solution in the outer layer is independent of both Re_θ and β, for sufficiently large Re_θ and β, when the velocity scale and length scale are taken as $u_\tau\sqrt{\beta}$ and $\Delta/\sqrt{\beta}$, respectively. We have solved Eq. (26) for the k–ϵ model (with the boundary conditions $k = \epsilon = 0$ for $\tilde{\eta} = 0$ and $\tilde{\eta} \to \infty$). As shown in Fig. 4a for the Reynolds shear stress, the solution of this equation is, indeed, the large β limit of the solutions of the defect-layer equation (23).

Figure 4b compares the solution with the k–ϵ model for the maximum of the Reynolds shear stress with experiments for $\beta \approx 1.9$ and 5.4 (Ref. 16), $\beta \approx 7$ (Ref. 17), and $\beta = 20$ (Ref. 12). The computations are made with different equations: the boundary-layer equations (1) and (2), the defect-layer equation (23), and the large-β defect-layer equation (26). The solution with the boundary-layer

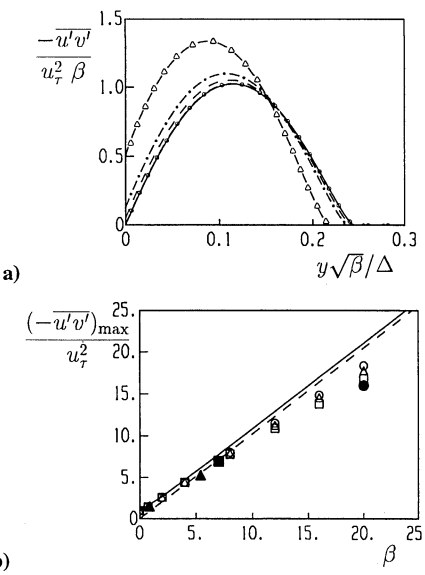

Fig. 4 Reynolds shear stress with the k–ϵ model for different β values: a) the similarity solution of Eq. (23) (△, $\beta = 2$; ·–·, $\beta = 8$; – – –, $\beta = 20$; ○, $\beta = 200$) and the $\beta \to \infty$ asymptote described by Eq. (26) (——); b) maximum of the Reynolds shear stress: filled symbols are experiments,[11,16,17] and open symbols are calculations with the boundary-layer equations (□, $Re_\theta = 5 \times 10^4$; △, $Re_\theta = 10^6$; ○, $Re_\theta = 10^8$); ——, similarity solution [Eq. (23)] and – – –, $\beta \to \infty$ asymptote [Eq. (26)].

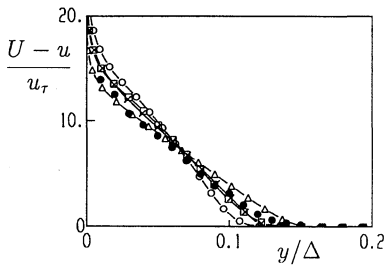

$\beta = 2$ (●, experiments by Clauser[1])

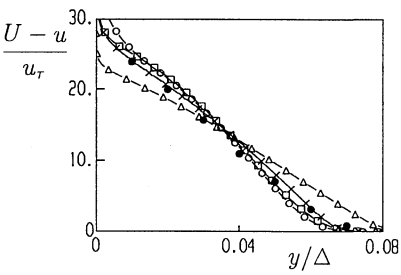

$\beta = 8$ (●, experiments by Clauser[1])

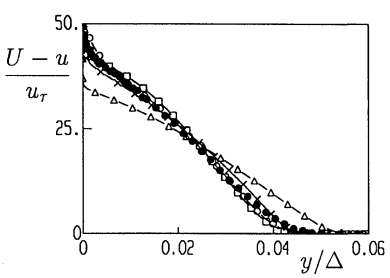

$\beta = 20$ (●, experiments by Skåre and Krogstad[12])

Fig. 5 Comparison between turbulence models (○, algebraic; △, k–ϵ; ×, k–ω; and □, DSM) and experiments for the streamwise velocity under different equilibrium conditions.

equations is shown for $Re_\theta = 5 \times 10^4$, 10^6, and 10^8. Figure 4b confirms again that the solution of the boundary-layer equations asymptotes to the solution of the defect-layer equation for $Re_\theta \to \infty$, whereas the latter also approaches an asymptote for $\beta \to \infty$. All experiments were performed at moderate Reynolds numbers, that is, between $Re_\theta = 10^4$ and 10^5. There is very good agreement between the computations and the experiments. For $\beta = 20$ there is a significant Reynolds number dependence, but the computational result shows close agreement with the experiment at $Re_\theta = 5 \times 10^4$, which is about the value where the experiments were performed.

The solution in the outer layer, as computed from the boundary-layer equations with different turbulence models, is compared with experiments in Fig. 5 for the streamwise velocity and in Fig. 6 for different turbulence quantities. The experiments are due to Clauser[1] ($\beta = 2$ and 8) and Skåre and Krogstad[12] ($\beta = 20$). The computational curves correspond to $Re_\theta = 10^6$ for $\beta = 2$ and 8, and to $Re_\theta = 5 \times 10^4$ for $\beta = 20$. All models, except for the k–ϵ model, closely predict the experimental streamwise velocity. All models also closely reproduce the experimental Reynolds shear stress, but the k–ϵ model somewhat overpredicts the boundary-layer thickness. The DSM predicts the structure parameter ($= -\overline{u'v'}/k$) best and is, in fact, very close to the new experiments for $\beta = 20$. The DSM also gives a quite good prediction of the Reynolds normal stresses.

With respect to the structure parameter, the experiments in Fig. 6 show that its value is almost constant and equal to about 0.3, across most of the outer-layer thickness. This implies that the Reynolds shear stress is proportional to the turbulent kinetic energy, as was also discussed by Bradshaw[16] based on his own experiments for a weaker adverse pressure gradient. Most turbulence models (including the k–ϵ model, the k–ω model, and the DSM) have chosen the model constants such that the proportionality with the structure parameter 0.3 is reproduced for flows in which the production of turbulence energy P_k ($= -\overline{u'v'}\partial u/\partial y$) equals the turbulent dissipation rate ϵ.

Table 2 Performance of turbulence models for $\beta = 20$ at $Re_\theta = 5 \times 10^4$

Model	c_f	H	G	m
Experiment[11]	0.000546	1.998	30.2	−0.220
Algebraic model	0.000463	1.938	31.8	−0.250
k–ϵ model	0.001335	2.757	24.7	−0.235
k–ω model	0.000638	2.141	29.9	−0.249
DSM	0.000584	2.275	32.8	−0.239

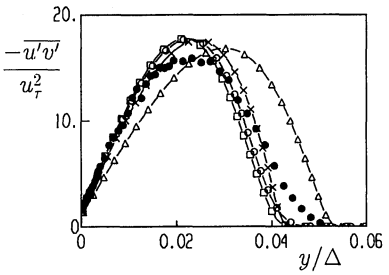

Reynolds shear stress

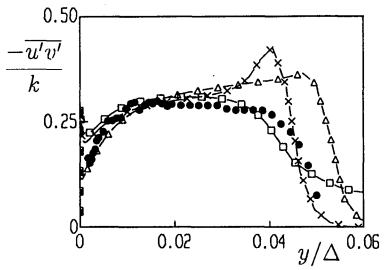

Structure parameter

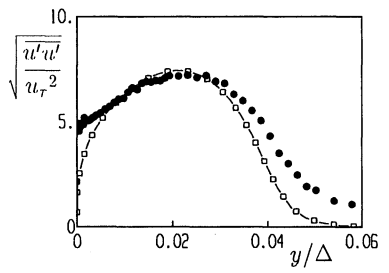

Reynolds normal stress along the wall

Fig. 6 Comparison between turbulence models (○, algebraic; △, k–ϵ; ×, k–ω; and □, DSM) and experiments for the turbulence in an equilibrium boundary layer with $\beta = 20$.

For example, the k–ϵ model has $-\overline{u'v'} = \nu_t \partial u/\partial y$, with $\nu_t = c_\mu k^2/\epsilon$. As the constant c_μ is set to 0.09, this gives $-\overline{u'v'}/k = 0.3$ when $P_k = \epsilon$.

A quantitative comparison between the models and the experiments for $\beta = 20$ at $Re_\theta = 5 \times 10^4$ is given in Table 2 for the wall-shear stress coefficient c_f, the shape factor H, the Clauser parameter G, and the m power in the outer-edge velocity. The poor performance of the k–ϵ model becomes most clear for the wall-shear stress coefficient, which is overpredicted by 145% compared to the experimental value. The DSM is superior, as it gives a value which is only 7% too large, whereas the algebraic model and the k–ω model give a slightly larger deviation of −15% and +17%, respectively. Also, for H and G, the largest deviation occurs with the k–ϵ model, which gives a value that is 38% too high and 18% too low, respectively. All models give about the same value for the m power, namely, from about −0.24 to −0.25, which is only slightly stronger than the experimental value of −0.22.

Conclusions

It was shown through numerically solving the boundary-layer equations up to $Re_\theta = 10^8$ that four types of turbulence models asymptote to the same classical scalings in the inner and outer layer for turbulent boundary layers under an adverse pressure gradient with an equilibrium parameter $\beta[= (\delta^*/\tau_w)(dp/dx)]$ between 0 and 200. The shape of the law of the wall in the inner layer is independent of β at large Re_θ. The solution in the outer layer asymptotes to the defect law described by the defect-layer equation of Tennekes and Lumley and not to the defect-layer equation of Wilcox (only for the zero-pressure gradient case, $\beta = 0$, both formulations are equal). (Note that this paper has been reviewed by, among others, Wilcox. The error described in the present paper will be corrected in the second edition of his book. Despite the error, Wilcox's conclusion that the k–ω model is more accurate than the k–ϵ model for boundary layers under an adverse pressure gradient remains valid.) The correctness of the formulation by Tennekes and Lumley was also verified by a series expansion in the small parameter u_τ/U. The similarity solution is approached slower for increasing β value; for example, even at $Re_\theta = 10^8$ (which may be considered as an upper limit for aircraft applications) the shape factor H can still be significantly above its asymptotic value $H = 1$. For increasingly large β, the defect-layer equation can be further simplified, which shows, for example, that the maximum Reynolds shear stress, when scaled with u_τ^2 is proportional to β. The power m in the outer-edge velocity that corresponds to a certain equilibrium boundary layer is not constant, but slowly decreases with increasing Reynolds number. A nonunique relation between the m power and the equilibrium parameter β is found for all four turbulence models, which is in agreement with the experimental findings of Clauser[1]; for example, the turbulence models show that equilibrium boundary layers with β values of about 3 and 20 are generated by the same outer-edge velocity. Comparison with experiments, particularly the recent experiments by Skåre and Krogstad[12] at $\beta = 20$, shows that among the tested turbulence models, the DSM is superior, but the algebraic model and the k–ω model are reasonably accurate. The k–ϵ model gives rather large deviations for strong adverse pressure gradients, where it considerably overpredicts the wall shear stress. However, only one specific form of the k–ϵ model was considered here (namely, the Launder and Sharma low Reynolds number k–ϵ model). Improvement of the k–ϵ model for adverse-pressure gradient flows can be expected when an additional source term is added to the ϵ equation. This was already demonstrated to give improvement for a nonequilibrium boundary layer.[13]

Acknowledgments

Part of this work was performed when the author was on leave at the Royal Institute of Technology in Stockholm, Sweden, with support from the Dutch Technology Foundation STW. Special thanks are due to Dan Henningson and Martin Skote for the stimulating discussions.

References

[1]Clauser, F. H., "Turbulent Boundary Layers in Adverse Pressure Gradients," *Journal of the Aeronautical Sciences*, Vol. 21, 1954, pp. 91–108.

[2]Von Kármán, T., "Mechanische Ähnlichkeit und Turbulenz," *Nachrichten der Konigliche Gesellschaft der Wissenschaften zu Göttingen*, Dieterich, Göttingen, Germany, 1930, pp. 58–76.

[3]Millikan, C. B., "A Critical Discussion of Turbulent Flows in Channels and Circular Tubes," *Proceedings of the 5th International Congress on Applied Mechanics*, edited by J. P. Dentalartog and H. Peters, Cambridge, England, UK, 1938, pp. 386–392.

[4]Coles, D., "The Law of the Wake in the Turbulent Boundary Layer," *Journal of Fluid Mechanics*, Vol. 1, 1956, pp. 191–226.

[5]George, W. K., and Castillo, L., "Boundary Layers with Pressure Gradient: Another Look at the Equilibrium Boundary Layer," *Near-Wall Turbulent Flows*, edited by R. M. C. So, C. G. Speziale, and B. E. Launder, Elsevier, New York, 1993, pp. 901–910.

[6]Cebeci, T., and Smith, A. M. O., *Analysis of Turbulent Boundary Layers*, Academic, New York, 1974.

[7]Launder, B. E., and Sharma, B. I., "Application of the Energy-Dissipation Model of Turbulence to the Calculation of Flow Near a Spinning Disk," *Letters in Heat and Mass Transfer*, Vol. 1, 1974, pp. 131–138.

[8]Wilcox, D. C., *Turbulence Modeling*, DCW Industries, Inc., La Cañada, CA, 1993, pp. 110–121.

[9]Hanjalić, K., Jakirlić, S., and Hadžić, I., "Computation of Oscillating Turbulent Flows at Transitional Re-Numbers," *Turbulent Shear Flows*, Vol. 9, edited by F. Durst, N. Kasagi, and B. E. Launder, Springer–Verlag, Berlin, 1995, pp. 323–342.

[10]Tennekes, H., and Lumley, J. L., *A First Course in Turbulence*, MIT Press, Cambridge, MA, 1972, pp. 186–188.

[11]Skåre, P. E., "Experimental Investigation of an Equilibrium Boundary Layer in Strong Adverse Pressure Gradient," Ph.D. Thesis, Rept. NTH 1994:179 (D), Dept. of Applied Mechanics, Thermo- and Fluid Dynamics, Univ. of Trondheim, Trondheim, Norway, 1994.

[12]Skåre, P. E., and Krogstad, P.-Å., "A Turbulent Equilibrium Boundary Layer near Separation," *Journal of Fluid Mechanics*, Vol. 272, 1994, pp. 319–348.

[13]Henkes, R. A. W. M., "Comparison of Turbulence Models for Basic Boundary Layers Relevant to Aeronautics," *Applied Scientific Research*, Vol. 57, No. 1, 1997, pp. 43–65.

[14]Spalart, P. R., "Direct Numerical Simulations of a Turbulent Boundary Layer up to $Re_\theta = 1410$," *Journal of Fluid Mechanics*, Vol. 187, 1988, pp. 61–98.

[15]Henkes, R. A. W. M., "Scaling of the Turbulent Boundary Layer Along a Flat Plate According to Different Turbulence Models," *International Journal of Heat and Fluid Flow* (submitted for publication).

[16]Bradshaw, P., "The Turbulent Structure of Equilibrium Boundary Layers," *Journal of Fluid Mechanics*, Vol. 29, Pt. 4, 1967, pp. 625–645.

[17]East, L. F., and Sawyer, W. G., "An Investigation of the Structure of Equilibrium Turbulent Boundary Layers," *Turbulent Boundary Layers: Experiment, Theory and Modelling*, AGARD CP-271, 1979, pp. 6.1–6.19.

F. W. Chambers
Associate Editor